Electronic Supplementary Information

Developing extended visible light responsive polymeric carbon nitrides for photocatalytic and photoelectrocatalytic applications

Sanjit Mondal[a], Gabriel Mark[a], Liel Abisdris[a], Junyi Li[a], Tirza Shmila[a], Jonathan Tzadikov[a], Michael Volokh[a], Lidan Xing[b], Menny Shalom*[a]

[a]*Department of Chemistry and Ilse Katz Institute for Nanoscale Science and Technology, Ben-Gurion University of the Negev, Beer-Sheva 8410501, Israel.*

E-mail: mennysh@bgu.ac.il

[b]*School of Chemistry, South China Normal University, Guangzhou 510006, China*

Detailed synthetic procedures

Materials: Melamine (M, 99%) was purchased from Alfa-Aeser. Ethylene glycol (EG, ≥99.5%) was supplied by Merck. Chloroplatinic acid (8 wt% in H_2O) was purchased from Sigma-Aldrich. Sulfuric acid (H_2SO_4, AR, 98%), was purchased from Carlo Erba. Potassium hydroxide pellets (KOH, AR, 85%) and sodium sulphate anhydrous (Na_2SO_4, AR, 99%) were purchased from Loba Chemie, India. Triethanolamine (TEOA, ≥99.0%) was bought from Glentham, UK. 2-propanol (IPA, AR) was purchased from Bio-Lab, Israel. FTO-coated glass (12–14 Ω sq^{-1}) was bought from Xop Glass company, Spain. Additionally, deionized water (DI) with 18.2 MΩ cm resistivity was obtained from a Millipore Direct-Q 3 water purification system. All chemicals were used as received without further purification.

Characterization: The structural analysis of all synthesized materials was carried out using powder X-ray diffraction patterns (PXRD) recorded using a PANalytical's Empyrean diffractometer which is equipped with a position sensitive detector X'Celerator. Data was recorded with a scanning time of ~15 min for 2θ ranging from 5° to 70° using Cu Kα radiation (λ = 1.54178 Å, 40 kV, 30 mA). Fourier-transform infrared spectroscopy (FTIR) was used to study the materials' functional groups using a Thermo Scientific Nicolet iS5 FTIR spectrometer (equipped with a Si ATR). UV–vis absorption spectroscopy (Cary 100 spectrophotometer, equipped with a diffuse reflectance accessory) and photoluminescence spectroscopy (Horiba Scientific FluroMax 4 spectrofluorometer) were used to study their optical properties. Morphology of the supramolecular precursor, final PCN powder, and PCN photoelectrodes were characterized by scanning electron microscopy (SEM) using a FEI Verios high-resolution SEM (equipped with a FEG source and a TLD detector operated at U_0 = 3.5 kV and I = 25 pA; to avoid charging effects, some samples were sputtered with ≤12 nm Pt using a Quorum Q150T ES system). In addition, transmission electron microscopy (TEM) images were recorded from a Tecnai T12 G2 TWIN microscope (U_0 = 120 kV). TEM specimens were prepared from an IPA dispersion of the sample obtained by ultrasonication and dropcasting onto a Cu TEM grid coated with holey carbon. Elemental analysis data for carbon, hydrogen, and nitrogen (CHN) was obtained using a Thermo Scientific Flash Smart elemental analyzer OEA 2000. Analytical TEM included energy-dispersive X-ray spectroscopy (EDS) analysis, carried out on a JEOL JEM 2100F TEM U_0 = 200 kV equipped with a JED-2300T EDS spectrometer. Scanning TEM (STEM) was conducted on the JEOL JEM 2100F using a GATAN 806 HAADF STEM detector. Nitrogen adsorption-desorption measurements and Brunauer-Emmet-Teller (BET) analyses were performed using a Quantachrome NOVAtouch NT LX3 system following a degassing procedure at 150 °C for 12 h.

Synthesis of melem: In a typical synthesis, 10 g of melamine powder was placed in a ceramic crucible covered with a lid and calcined at 400 °C for 12 h, in a muffle furnace in the air. A heating ramp of 5 °C min^{-1} was applied from room temperature to the target temperature was used. Pale-yellow colored solids were obtained and further ground using an agate mortar-and-pestle to obtain fine powder of melem for subsequent use.

Synthesis of supramolecular precursor: 3 mmol of melem (mlm) and 3 mmol of melamine (M) powder were added into 60 mL of an aqueous solution containing various ethylene glycol (EG) concentrations (0, 16, 32, and 50 v%) and the mixture was then shaken for 12 h. The above mixture was transferred into PTFE-lined autoclave and placed into an oven at 160 °C for 20 h. The autoclave was cooled naturally to room temperature and the resulting white slurry,

a supramolecular precursor (P_{M+mlm}), was obtained by centrifugation. For the comparison study, P_M and P_{mlm} were also synthesized by treating hydrothermally at 160 °C for 20 h (in 32 v% EG aqueous solution) either only melamine or only melem.

Synthesis of nanostructured CN (for use as a photocatalyst): The obtained supramolecular precursors (P_M, P_{mlm}, and P_{M+mlm}) were washed once with deionized water and dried under vacuum at 60 °C overnight. Next, the supramolecular powder was transferred into a ceramic crucible covered with a lid and placed in a muffle furnace at 550 °C for 4 h with 2 °C min^{-1} heating rate under aerial condition. The sample was naturally cooled at room temperature. Light-brown powder was obtained.

Photoelectrodes preparation procedure: To construct a CN photoelectrode, the supramolecular precursor obtained after the hydrothermal treatment was centrifuged at 6000 rpm and 0.5 g of the settled slurry was ground until a homogeneous viscous paste is obtained (without addition of EG in this stage). This paste was doctor-bladed onto a clean FTO substrate with thickness of two scotch tape (3M) layers used to achieve a homogeneous coating, and subsequently dried at *ca.* 85 °C on a hot plate. The doctor-bladed FTO substrates were placed inside a closed glass test tube with 16 mm diameter. Two electrodes were kept inside the test tube and 0.5 g of melamine powder was placed at the bottom of the test tube and sealed with the aluminum foil.[1] Next, the samples were calcined at 550 °C for 4 h under continuous N_2 flow (from room temperature to the target temperature a heating rate of 5 °C min^{-1} was used).

Photocatalytic hydrogen evolution reaction (HER): Photocatalytic HER experiments were carried out under Ar (99.999%) atmosphere at 25 °C, controlled by a circulating cooling system. Typically, a 30 mL quartz reaction vessel with 10 mL of an aqueous reaction aliquot containing 10 v% of TEOA as a sacrificial reagent and 3.7 mg of nanostructured CN catalyst in a H_2PtCl_6 aqueous solution (loading of 3 wt.% Pt relative to CN mass) was added, followed by sonication for 2–3 min to yield a homogeneous suspension. The reaction vessel was then placed in thermostatically-controlled water bath. The reaction mixture was first purged with Ar(g) for 30 min (constant stirring at 600 rpm). A white LED array (Bridgelux BXRA-50C5300, 100 W, $\lambda > 410$ nm) was used as the illuminating source. Upon light illumination, 50 µL of the generated H_2(g) in the headspace of the reaction vessel was collected using a gas-tight syringe at regular intervals and analyzed by gas chromatography (Agilent 7820 GC system). The experimental error in the rate of H_2 evolution was within 7%. To study the stability of the material, after the 1st cycle, the same solution was degassed and then the 2nd cycle of the reaction performed. The apparent quantum efficiency (AQE) was measured using a sealed reactor with an Ar-line connected to an Agilent 7820 GC system. Ar was purged continuously for 15 min before turning on the light source. A Thorlabs mounted LED (wavelengths of 395, 405, 430, 455, 495, 525, and 555 nm) was used for the AQE measurement. The amount of produced H_2 was measured automatically by sampling every 11 min. The AQE was calculated using the following equation:

$$\mathrm{AQE} = \frac{2 \times \text{Number of evolved } \mathrm{H_2} \text{ molecules}}{\text{Number of incident photons}} \times 100\%$$

PEC and electrochemical measurements: All the photoelectrochemical measurements were carried out using a standard three-electrode system on a PalmSens4 potentiostat. A Pt foil (1.0

cm^2) and Ag/AgCl (saturated KCl) were used as the counter- and reference-electrode, respectively. 0.1 M KOH aqueous solution, (pH ~13.1) or 0.1 M KOH aqueous solution containing 10 v% triethanolamine were used as the electrolyte for the photocurrent measurements. In addition, 0.5 M H_2SO_4 and 0.5 M Na_2SO_4 aqueous solutions were also used for photocurrent measurement in acidic and neutral environments, respectively. The obtained potentials were converted to the reversible hydrogen electrode (RHE) scale using the following equation:

$$V_{RHE} = V_{Ag/AgCl} + 0.0591 \times pH + 0.197.$$

Photocurrents were recorded at 1.23 V bias *vs.* RHE using illumination from a solar simulator (Newport 300 W ozone free Xe arc lamp, equipped with water and air mass AM 1.5G filters) calibrated to a 1-sun illumination (100 mW cm^{-2} power density, calibration Newport power meter model 919-P). For incident photon-to-current conversion efficiency (IPCE) calculations:

$$\text{IPCE (\%)} = \frac{J\ (\text{mA cm}^{-2}) \cdot 1240}{\lambda(\text{nm}) \cdot I_{\text{incident}}(\text{mW cm}^{-2})} \times 100\%$$

where J is the measured photocurrent density, λ is the wavelength of the incident monochromic light and $I_{incident}$ is the incident illuminating power density.

Table S1. Interaction energies values calculated from density functional theory (DFT) simulations. (All calculations were performed using the G16 software package. The equilibrium structures were optimized by B3LYP method in conjunction with the 6 311++G (d) basis set.)

Interaction of different monomers with EG	Calculated interaction energy (E_{int}, kJ mol^{-1})
M–EG–M	–75.9
M–EG–mlm	–81.7
mlm–EG–mlm	–86.9

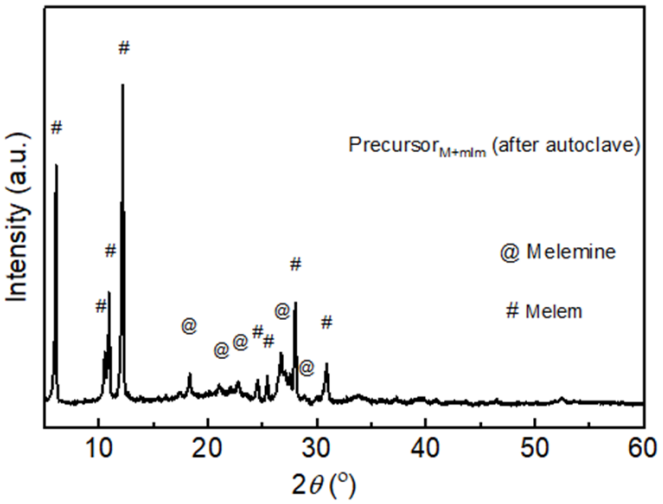

Fig. S1 XRD pattern of the P_{M+mlm}.[2] (Melamine PDF# 391950 and for melem reference is provided)

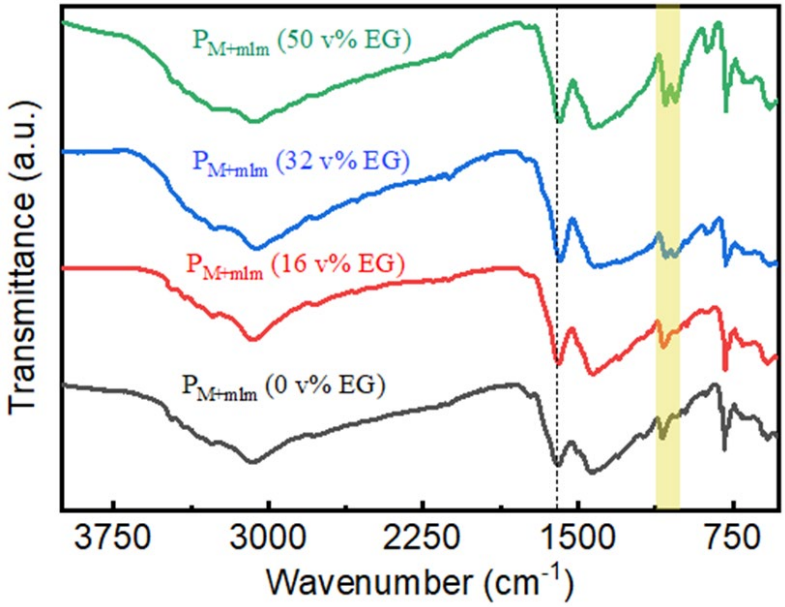

Fig. S2 FTIR spectra of P_{M+mlm} samples with various amount of EG (volume precent of EG in water, *i.e.*, from 0 v% to 50 v%) during hydrothermal treatment. Spectra are vertically offset for clarity.

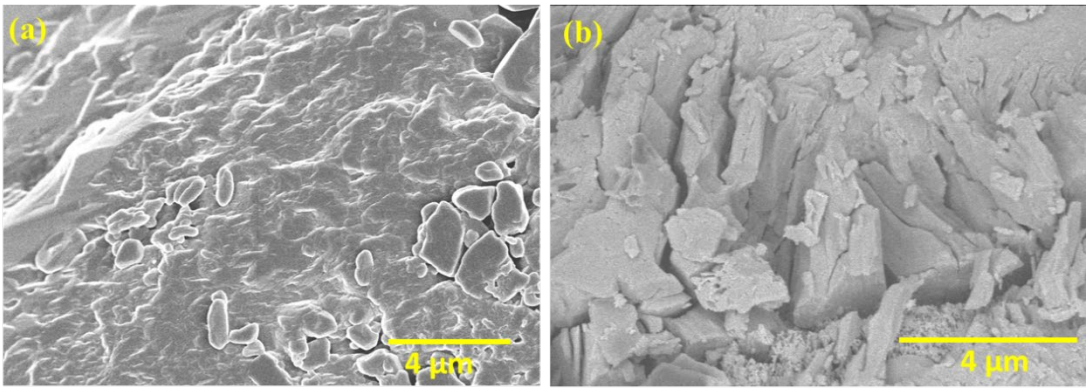

Fig. S3 SEM image of untreated (a) melamine and (b) melem.

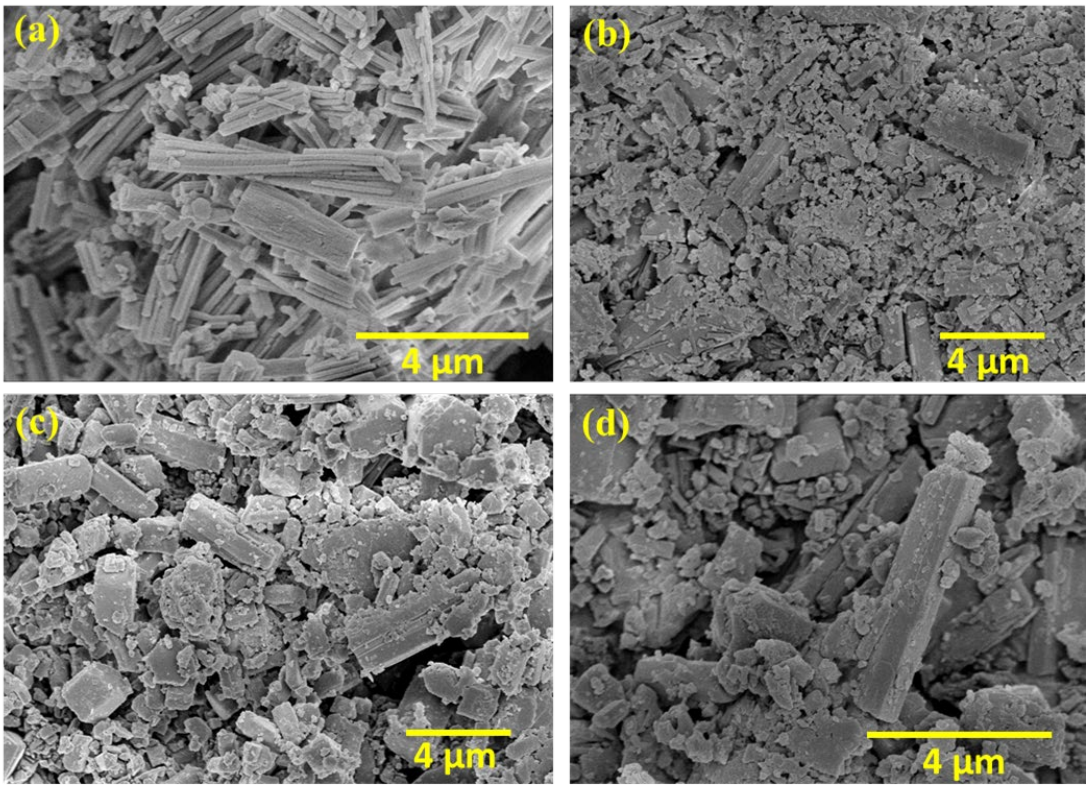

Fig. S4 SEM images of hydrothermally treated precursors of P_{M+mlm} with various amounts of EG content: (a) no EG (*i.e.*, 0 v%), (b) 16 v% EG, (c) 32 v% EG, and (d) 50 v% EG.

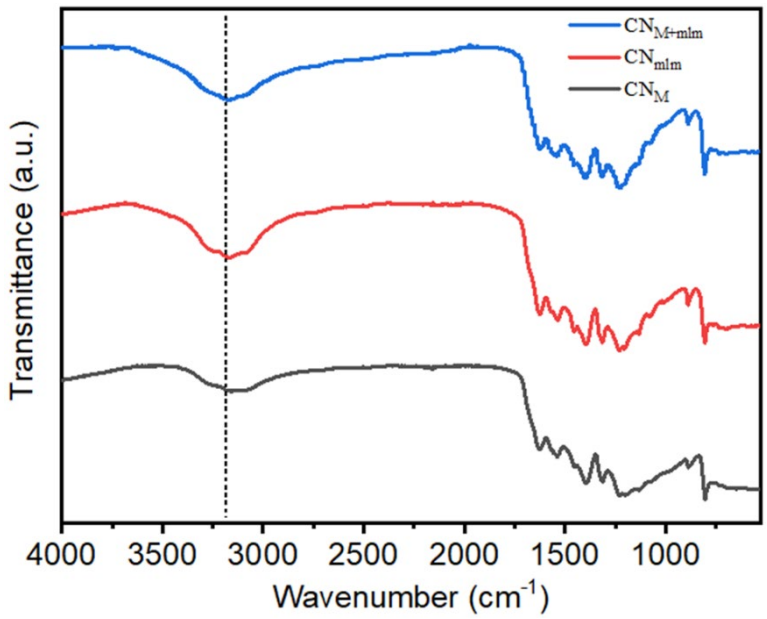

Fig. S5 FTIR spectra of the CN_M, CN_{mlm}, and CN_{M+mlm} samples. Spectra are vertically offset for clarity.

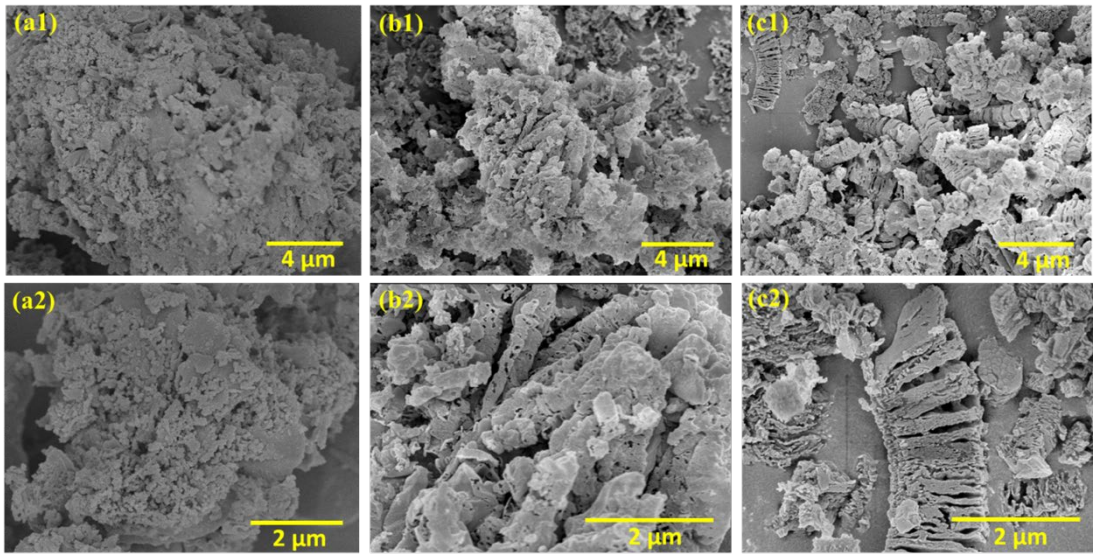

Fig. S6 SEM images at two magnifications of the final CN powders. (a1,a2) CN_M, (b1, b2), CN_{mlm}, and (c1, c2) CN_{M+mlm}.

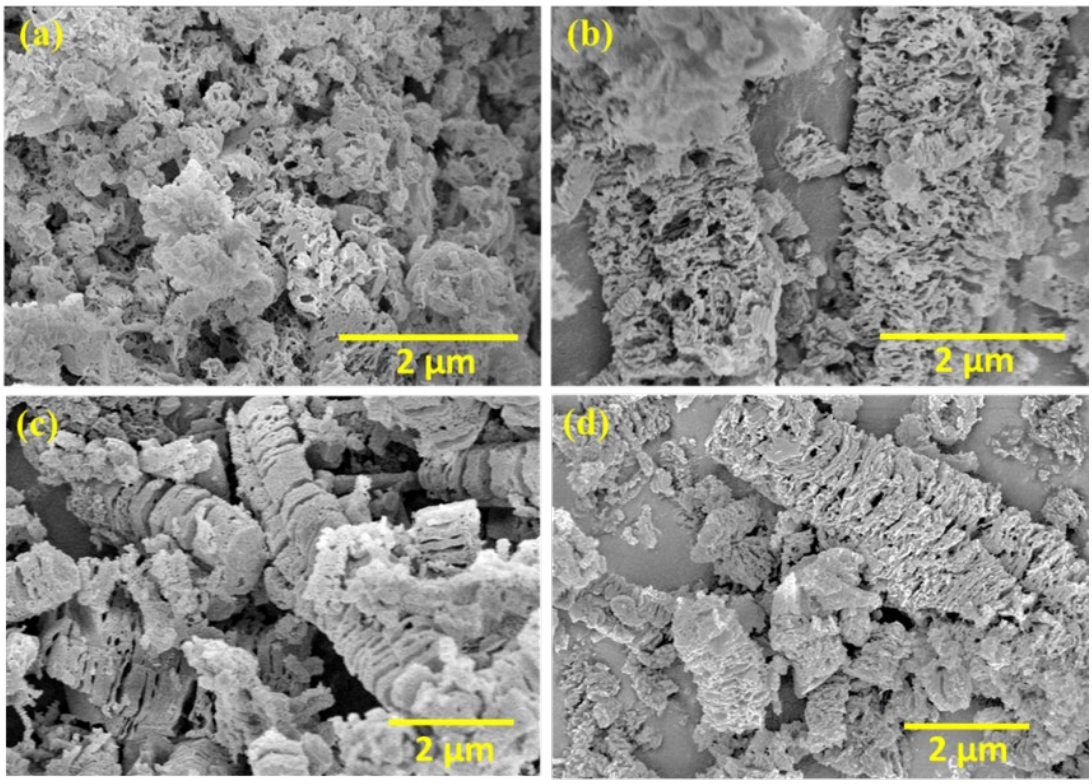

Fig. S7 SEM images of final CN_{M+mlm} samples prepared by calcination of P_{M+mlm} precursor in varying EG content: (a) no EG, (b) 16 v% EG, (c) 32 v% EG, and (d) 50 v% EG.

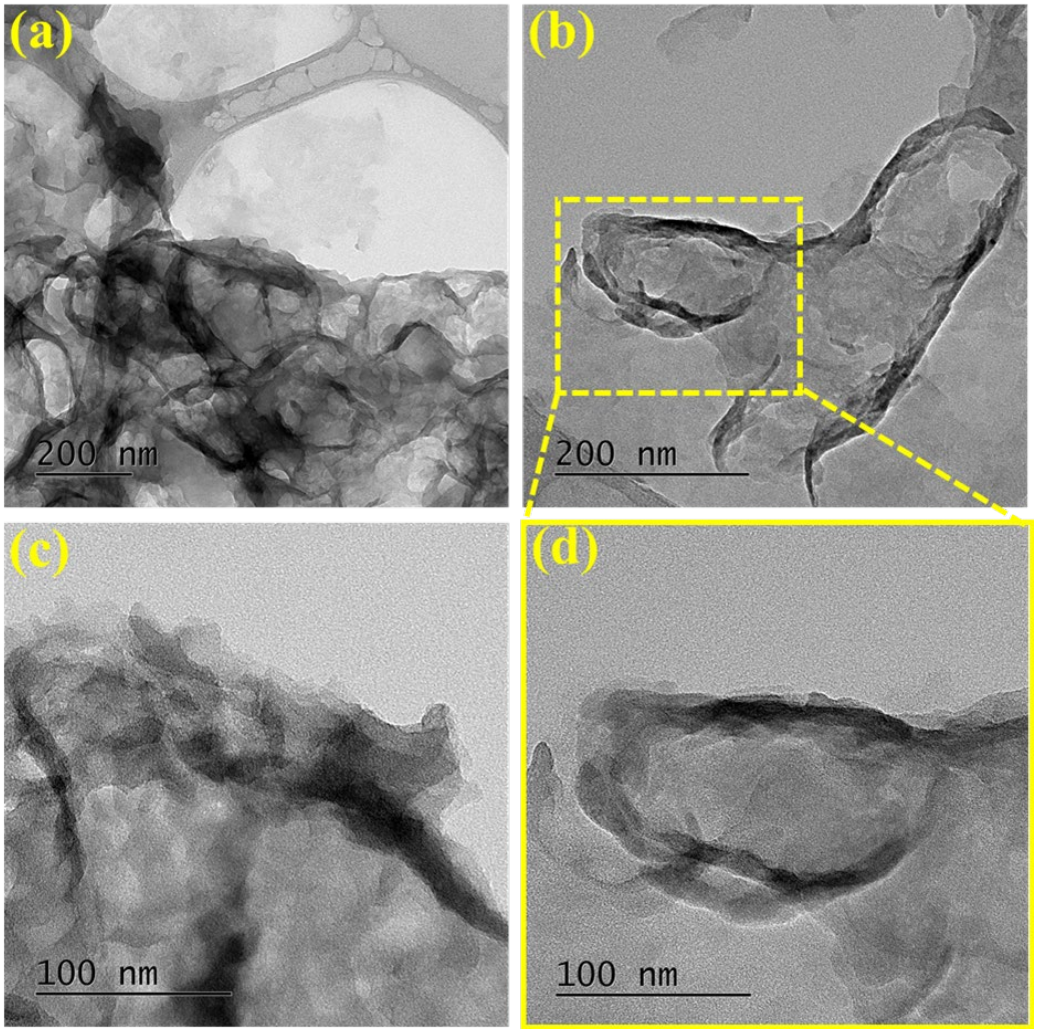

Fig. S8 TEM images of CN_{M+mlm} at different magnifications.

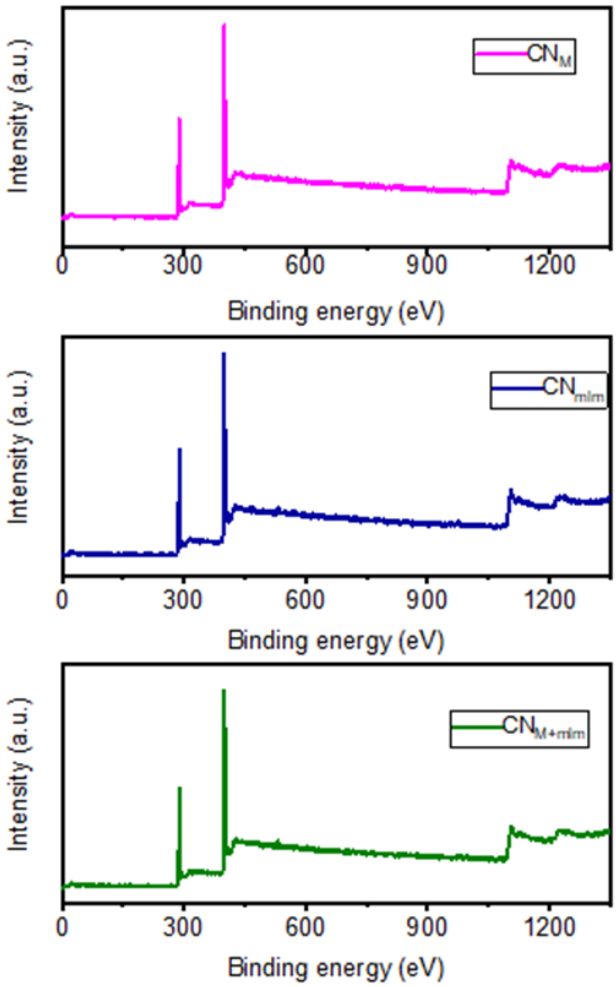

Fig. S9 XPS survey spectra of CN_M, CN_{mlm}, and CN_{M+mlm} samples.

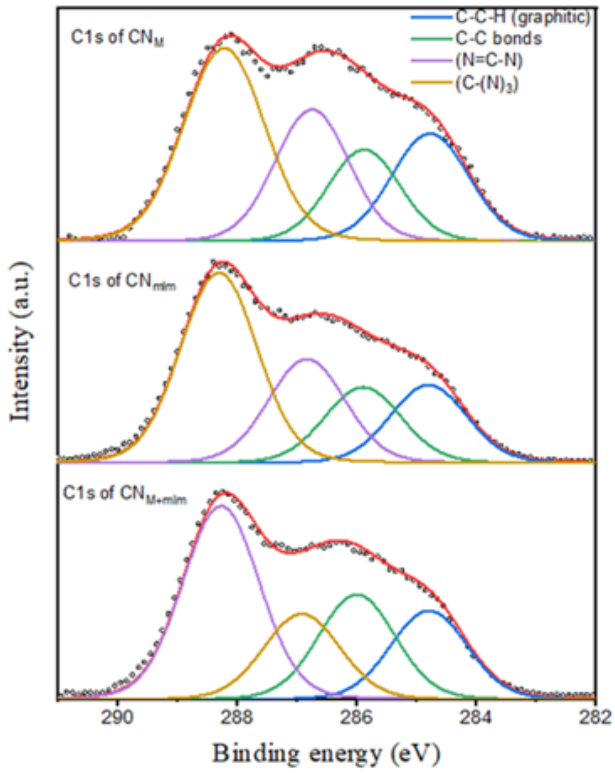

Fig. S10 C1s XPS spectra of CN_M, CN_{mlm}, and CN_{M+mlm} samples (etch time 60 s).

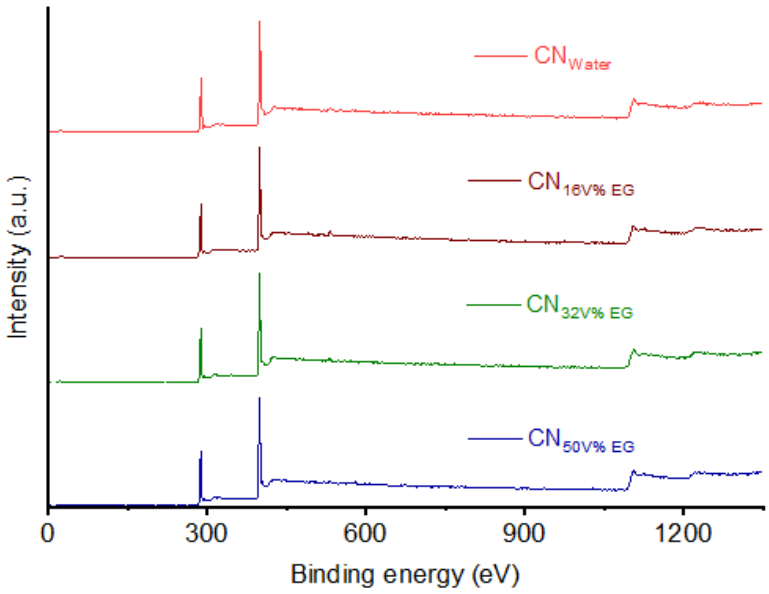

Fig. S11 XPS survey spectra of CN_{M+mlm} with various EG content.

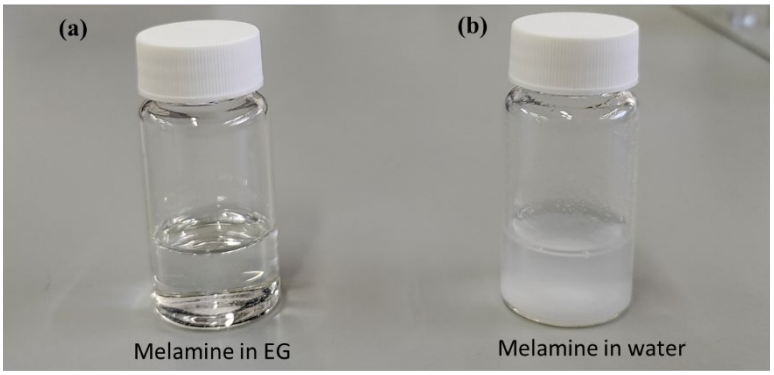

Fig. S12 Digital photographs of melamine in (a) ethylene glycol, (b) water.

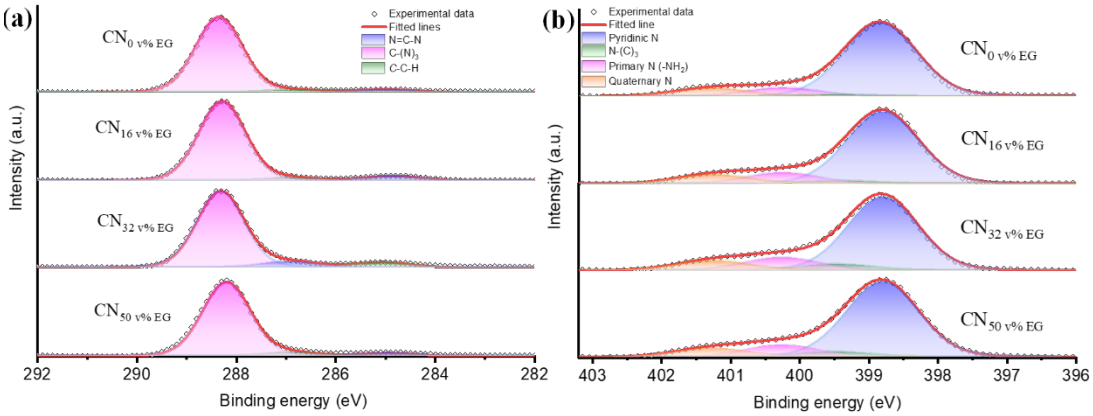

Fig. S13 (a) C1s and (b) N1s XPS spectra of CN_{M+mlm} with various EG content.

Table S2. Relative ratios of groups in N 1s XPS spectra for CN with various EG content.

Sample	Py	NH_2	NH	Q
CN_{Water}	80.1	1.60	9.36	8.82
$CN_{16V\%\ EG}$	75.2	3.25	11.82	9.70
$CN_{32V\%\ EG}$	70.6	6.30	13.18	10.0
$CN_{50V\%\ EG}$	73.5	5.15	12.36	8.99

Table S3. Elemental analysis data, atom% of (a) CN_M, CN_{mlm}, and CN_{M+mlm}. (b) Elemental analysis data of CN_{M+mlm} samples with various amount of EG during the hydrothermal treatment.

(a)

Sample	N (%)	C (%)	H (%)	O (%)	C/N ratio
CN_M	46.40	30.39	21.15	2.49	0.654
CN_{mlm}	44.28	29.68	22.59	3.43	0.670
CN_{M+mlm}	43.53	29.83	23.44	3.18	0.685

(b)

Sample	N (%)	C (%)	H (%)	O (%)	C/N ratio
CN_{M+mlm} (0 v% EG)	45.06	29.25	22.72	2.95	0.649
CN_{M+mlm} (16 v% EG)	44.57	29.36	22.96	3.09	0.659
CN_{M+mlm} (32 v% EG)	43.53	29.83	23.44	3.18	0.685
CN_{M+mlm} (50 v% EG)	44.97	30.38	21.93	2.70	0.675

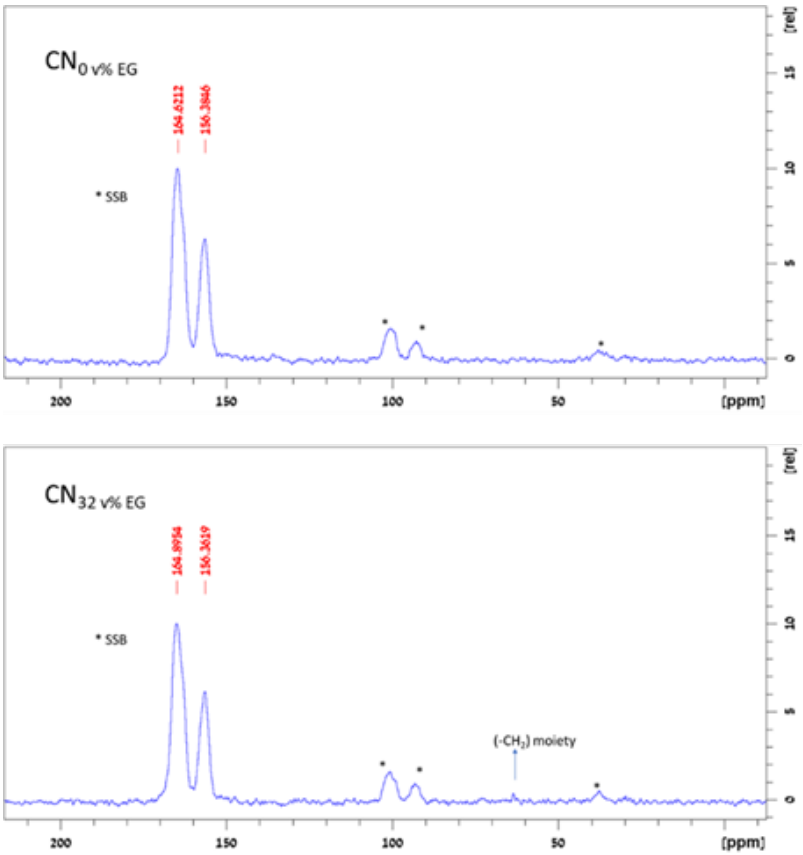

Fig. S14 Solid state ^{13}C NMR of $CN_{0v\%\ EG}$ and $CN_{32v\%\ EG}$ samples.

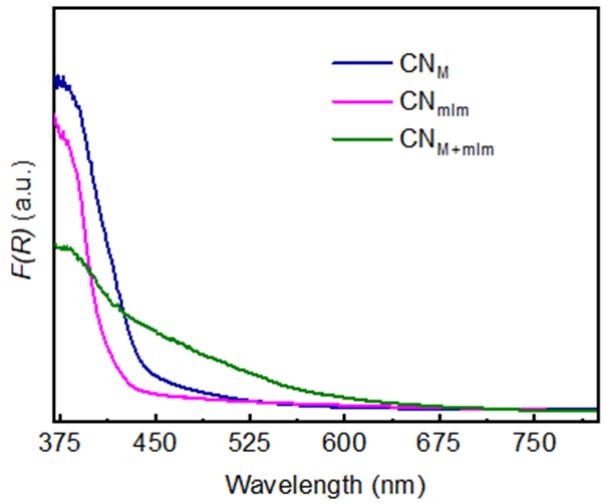

Fig. S15 UV–vis DRS spectra of CN_M, CN_{mlm}, and CN_{M+mlm} samples.

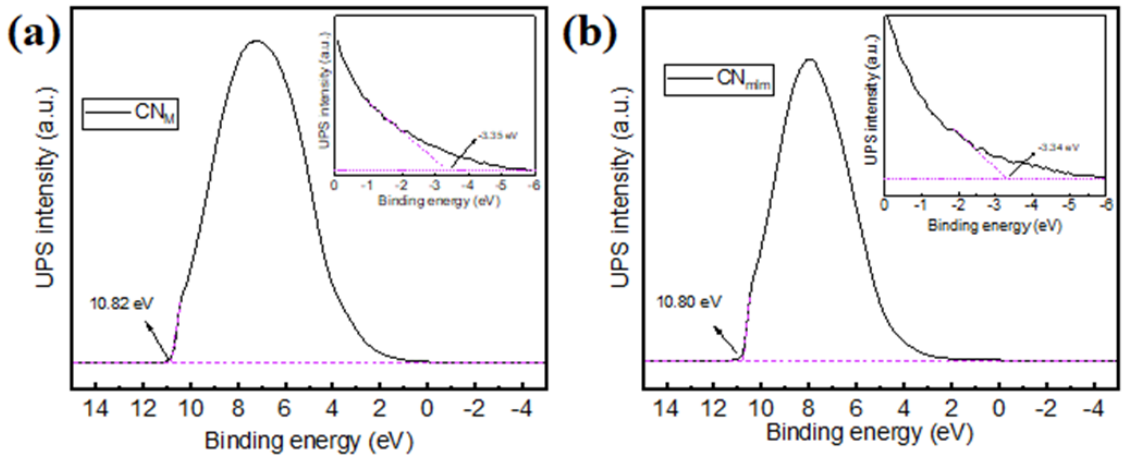

Fig. S16 UPS valance band spectrum of (a) CN_M and (b) CN_{mlm}.

The VB energies (E_{VB}) of CN_M, CN_{mlm}, and CN_{M+mlm} were calculated to be 7.04 eV, 7.07 eV, and 6.37 eV, respectively, by subtracting the width of HeI-UPS spectra from the excitation energy (E_{ex} = 21.21 eV). The CB energy (E_{CB}) is thus estimated at 4.11 eV, 4.06 eV, and 3.82 eV, respectively, from $E_{VB} - E_g$(optical). The E_{VB} and E_{CB} values of CN_M, CN_{mlm}, and CN_{M+mlm} (eV) could be converted to an electrochemical energy potential using a standard reference scale where 0 V *vs.* RHE (reversible hydrogen electrode) equals 4.44 eV *vs.* E_{vac} (vacuum level).[3] The calculated E_{VB} *vs.* RHE of CN_M, CN_{mlm}, and CN_{M+mlm} are 2.61, 2.62 and 2.20 V, respectively.

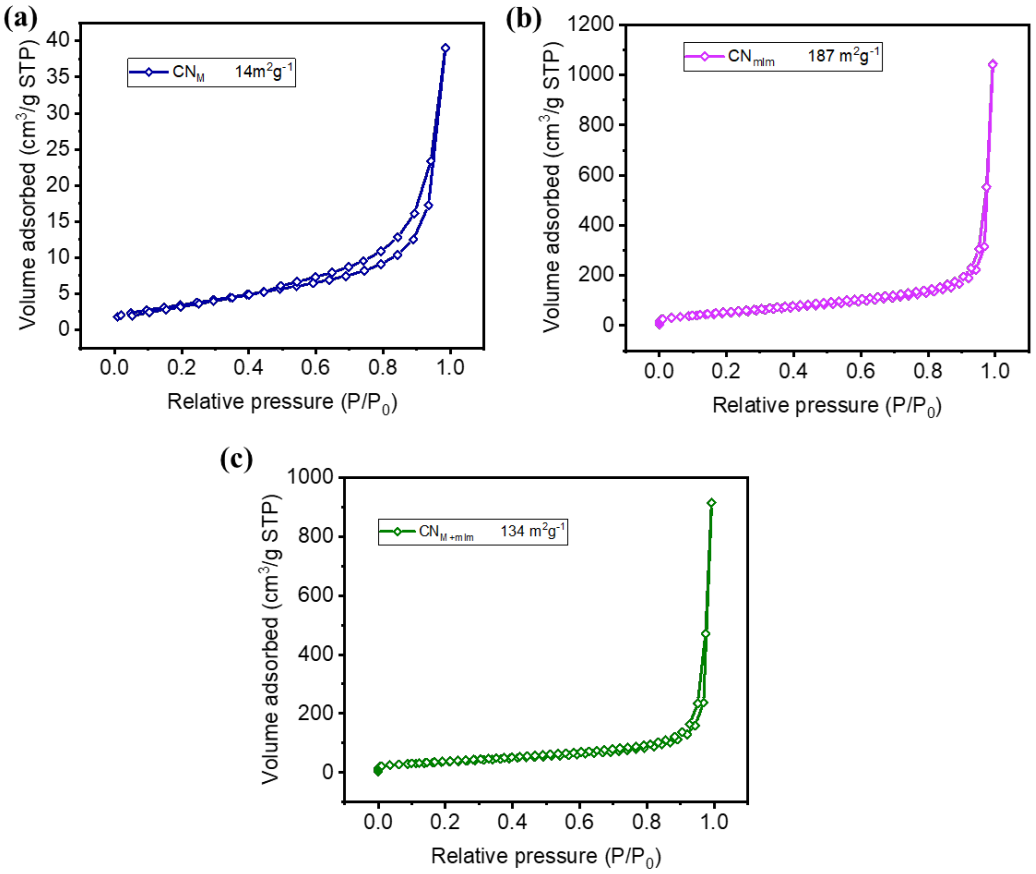

Fig. S17 Nitrogen sorption isotherms (77 K) and specific surface area (S_A) estimation using the BET model for (a) CN_M [S_A = 14 m^2 g^{-1}], (b) CN_{mlm} [S_A = 187 m^2 g^{-1}], and (c) CN_{M+mlm} [S_A = 134 m^2 g^{-1}].

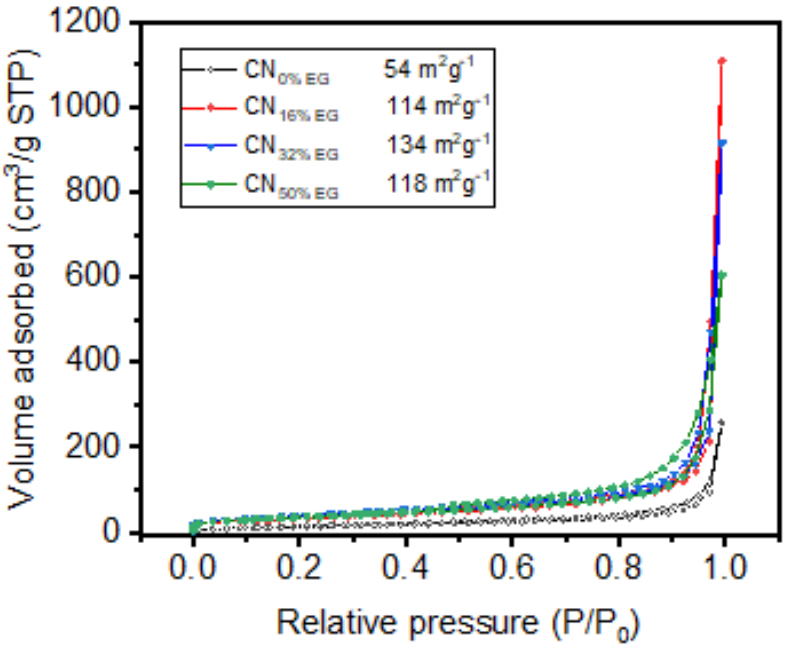

Fig. S18 Nitrogen sorption isotherms (77 K) and specific surface area (S_A) estimation using the BET model for CN_{M+mlm} prepared using variable EG content.

Table S4. HER photocatalytic activity of CN-based materials.

Photocatalyst	Method	Light source	Catalyst mass	BET S_A ($m^2\ g^{-1}$)	Experimental conditions	HER rate ($\mu mol\ g^{-1}\ h^{-1}$)	AQE (%)	Ref.
CN_{M+mlm}	Melamine-EG-mlm supramolecular assembly via autoclave treatment followed by calcination.	100 W white LED, $\lambda > 410$ nm	3.8 mg	131	3 wt. % Pt, 10 vol. % TEOA	23120	19.2 @ 395 nm	This work
CN-2-Cl-mlm	Melem-halogen supramolecular assembly, followed by thermal condensation.	100 W white LED, $\lambda > 410$ nm	7.5 mg	78.5	3 wt. % Pt, 10 vol. % TEOA	8952	9.05 @ 415 nm	[4]
CN-MS	Supramolecular assembly with a thiol-containing monomer, followed by thermal condensation.	50 W white LED, $\lambda > 410$ nm)	15 mg	25.61	3 wt. % Pt, 10 vol. % TEOA	838	1.6 @ 405 nm	[5]
CN-3MeTAP	Melem-based supramolecular assembly, followed by thermal condensation.	100 W white LED, $\lambda > 410$ nm	15 mg	100.0	3 wt. % Pt, 10 vol. % TEOA	8075	15.2 @ 405 nm	[6]
CN-CMT_2	Supramolecular assembly followed by thermal condensation with an additive.	100 W white LED, $\lambda > 410$ nm	15 mg	–	3 wt. % Pt, 10 vol. % TEOA	1757	6 @ 405 nm	[7]

soluble g-C_3N_4 (SCN) nanosheets	Melamine thermal condensation and a freeze-drying process.	Four 3 W and 420 nm low-power LEDs	50 mg	–	1 wt. % Pt, 10 vol. % lactic acid	359.6	–	[8]
$CNU_{0.075}$	Dicyandiamide and uracil in a hydrothermal method followed by thermal condensation.	300 W Xe arc lamp	50 mg	11.41	3 wt. % Pt, 10 vol. % TEOA	4243.62	–	[9]
PCNS-2	Thiourea and NH_4Cl thermal condensation.	300 W Xe lamp + cutoff filter (λ > 420 nm)	15 mg	126.7	10 vol. % TEOA	~340	–	[10]
NCDs/DCN	Citric acid and urea with a hydrothermal method.	300 W Xe lamp + cutoff filter, λ > 420 nm)	50 mg	51.77	In 50 mL water the photocatalyst and 0.5 mg of dispersed RhB.	626.93	–	[11]
CNBYO-2	Urea thermal condensation. $BiYO_3$ was prepared by a hydrothermal method. Then electrostatic self-assembly.	PLS-SXE 300UV Xe arc lamp + cutoff filter (λ > 400 nm)	20 mg	55.78	10 vol. % TEOA	37.65	–	[12]

Exfoliated and g-C_3N_4 mixture	g-C_3N_4 urea via thermal condensation. Exfoliation with a mixture of nitric and sulfuric acids.	four 365 nm LEDs (21 mW cm^{-2} total)	–	–	2 wt. % Pt, 10 vol. % TEOA	3810	5.2 @ 405 nm	[13]
R-CN-350	CVD method using melamine as the precipitating precursor. SiO_2 the template, removed with 4 M NH_4HF_2.	Xe lamp (300 W) + 420 nm filter	10 mg	29.9	3 wt. % Pt, 10 vol. % TEOA	1900	–	[14]
H-PHI	Dicyandiamide, KSCN, and potassium melonate penta-hydrate thermal condensation under inert atmosphere, followed by HCl etching.	Xe arc-lamp (300 W) equipped with a 1.5 Global AM filter working at 100 mW cm^{-2}	14–20 mg	–	2 wt. % Pt, 10 vol. % EtOH	3364	–	[15]
CN-$Mo_{0.2}$	Uracil ammonium molybdate and melamine assembly through a hydrothermal method. Thermal condensation.	Xe lamp (300 W) + 420 nm cutoff filter	50 mg	56	3 wt. % Pt, 10 vol. % TEOA	2008.9	3.72 @ 420 nm	[16]
Ag-N_2C_2/CN	Melamine, $AgNO_3$, citric acid, and cyanuric acid supramolecular assembly, then thermal condensation.	300 W Xe lamp + long pass cutoff	20 mg	105.02	10 vol. % TEOA	1866	–	[17]

		filter (λ > 420 nm)						
2AP-CN-15	Urea and 2-aminopyridine thermal condensation.	300 W Xe lamp + 420 nm cutoff filter	20 mg	135.663	3 wt. % Pt, 20 vol. % TEOA	6317.5	20.1 @ 420 nm	[18]
A-V-g-C_3N_4	Dicyandiamide in a high-temperature treatment and two-step thermal exfoliation process.	PLS-SXE300CBF Xe arc + 420 nm cutoff filter	50 mg	267.1	1 wt. % Pt, 10 vol. % TEOA	3700	14.98 @ >420	[19]
1.5CCN650	Melamine and KF assembly in ethanol, then thermal condensation.	Xe lamp + 420 nm filter 100 mW cm^{-2}	10 mg	–	3 wt. % Pt, 10 vol. % TEOA	1889	4.1	[20]

$BF_{0.065}$-g-C_3N_4	Basic fuchsin and urea copolymerization method, followed by thermal condensation.	300 W Xe lamp + 420 nm cutoff filter	50 mg	87.19	3 wt. % Pt, 10 vol. % TEOA	1619.0	–	[21]
MoS_2/g-C_3N_4 nanosheets	g-C_3N_4 nanosheets and ammonium tetra-thiomolybdate in DMF via solvent-thermal method.	100 W Xe lamp + cutoff filter (λ > 420 nm)	50 mg	94.87	0.1 M TEOA	1155	6.8 @ 420 nm	[22]
CN-10	Dicyandiamide and NaCl assembly in ethanol and water, followed by thermal condensation.	300 W Xe lamp + UV-cutoff filter (λ > 400 nm).	50 mg	16.71	3 wt. % Pt, 25 vol. % lactic acid	459	2.2 @ 420 nm	[23]
CN-MP0.1	Urea and 2,6-dimethylmorpholine through direct co-polymerization route, followed by thermal condensation.	300 W Xe lamp (at 15 cm distance) by using suitable	50 mg	160.60	3 wt. % Pt, 10 vol. % TEOA	2936.2	–	[24]

		extended permit cut-off (λ > 420 nm)						
PCN-SA-d	Succinic acid in liquid urea with thermal condensation.	Xe lamp equipped with a CEL-UVIRCUT 420 cutoff filter ($\lambda \geq$ 420 nm), ~425 mW cm^{-2}	20 mg	68.1	3 wt. % Pt, 10 vol. % TEOA	8520	5.6 @ 420 nm	[25]
TSC−550	Thiosemicarbazide (TSC) powder thermal condensation.	Xe lamp (300 W) + UV-cutoff filter (λ > 420 nm)	50 mg	95.2	3 wt. % Pt, 10 vol. % TEOA	9768	14.6 @ 425 nm	[26]
Nic-CN	Melamine and nicotinic acid assembly through hydrothermal method followed by thermal condensation.	300 W Xe lamp (λ > 420 nm)	20 mg	40.95	1 wt. % Pt, 10 vol. % EtOH	6310	6.81 @ 420 nm	[27]

$PCN\text{-}BPT_{15}$	Urea and 1-benzyl-3-phenylthiourea (BPT), thermal condensation.	300 W Xe lamp (λ > 420 nm)	50 mg	117.4	1 wt. % Pt, 20 vol. % TEOA	2500	24.2 @ 420 nm	[28]
$CN\text{-}M_{10}TAP_{0.05}$	2,4,6- triaminopyrimidine (TAP) and melem thermal condensation	100 W LED lamp (λ > 410 nm)	15 mg	99.7	3 wt. % Pt, 10 vol. % TEOA	10160	20.0 @ 405 nm	[29]

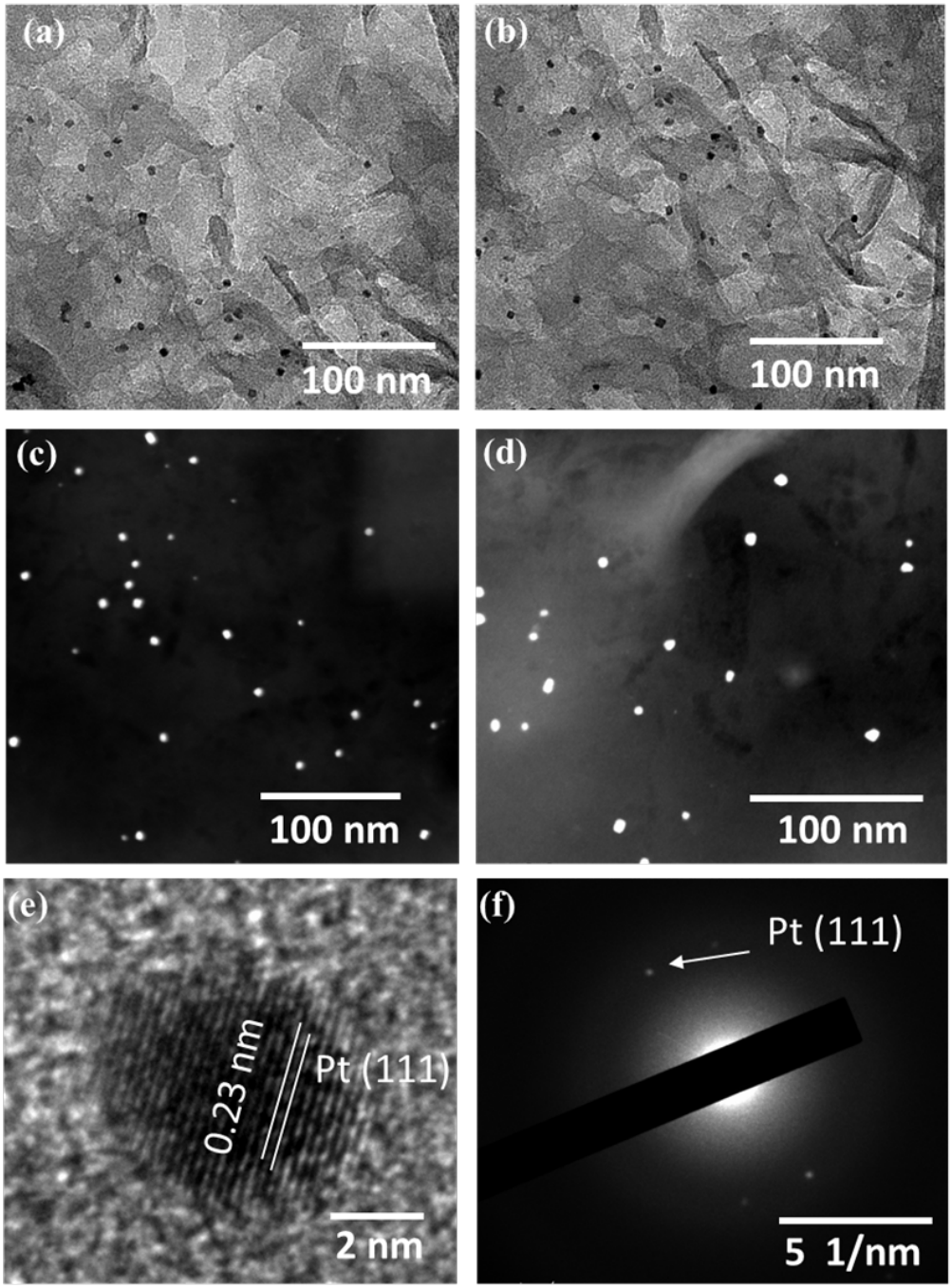

Fig. S19 TEM analysis of CN_{M+mlm} catalysts after the 5th HER cycle: (a, b) TEM images, (c, d) STEM images, (e) HRTEM image, and (f) Selected area electron diffraction (SAED) pattern.

Fig. S20 Photograph of CN_{M+mlm} in water showing high dispersibility of CN.

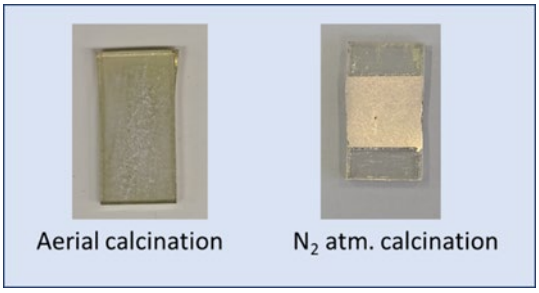

Fig. S21 Digital photographs of CN_{M+mlm} photoelectrodes obtained after calcination in air (left) and under N_2 atmosphere (right).

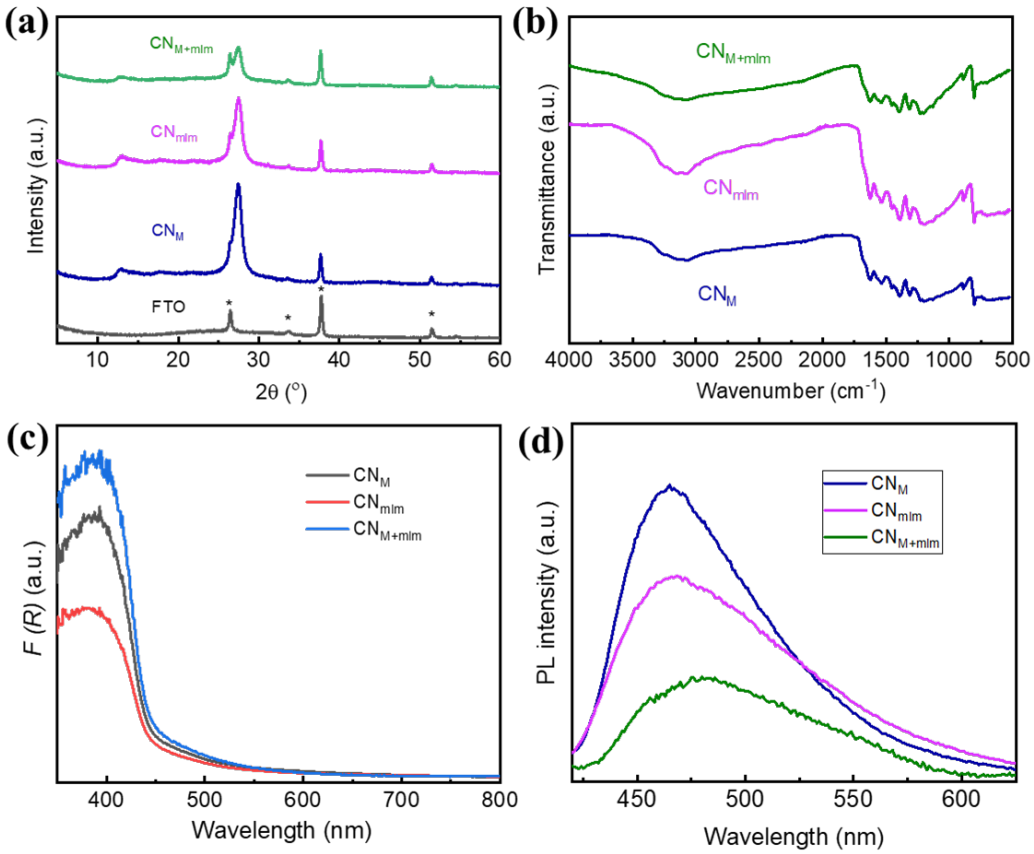

Fig. S22 CN_M, CN_{mlm}, and CN_{M+mlm} on FTO-coated glass electrodes characterization. (a) XRD, (diffraction signals of the FTO stem mainly from SnO_2 (marked with an *), JCPDS 77-0447). (b) FTIR, (c) UV–vis DRS, (d) Photoluminescence emission spectra (excitation wavelength 375 nm).

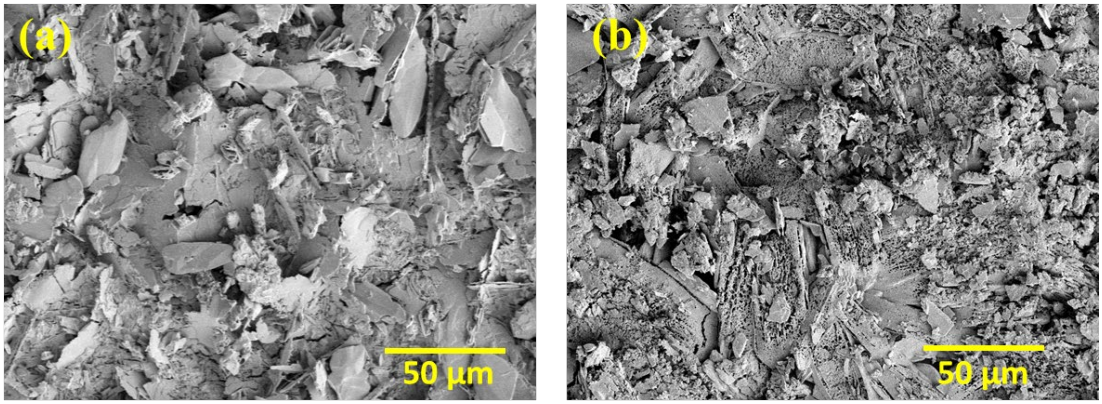

Fig. S23 SEM images of (a) CN_M and (b) CN_{mlm} electrodes.

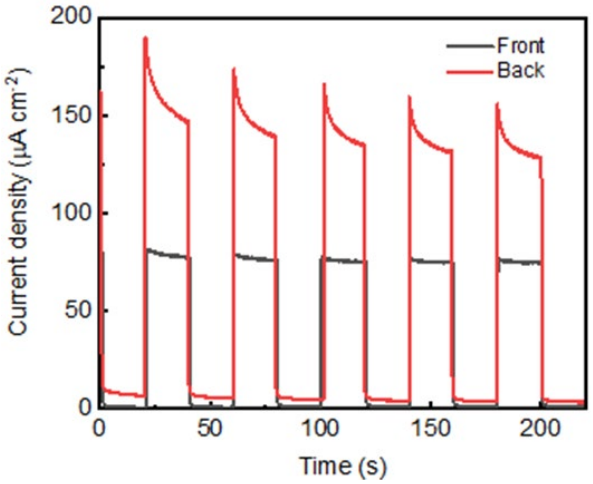

Fig. S24 Front- and back-illuminated chronoamperometry (on/off illumination cycles) of CN_{M+mlm} electrode.

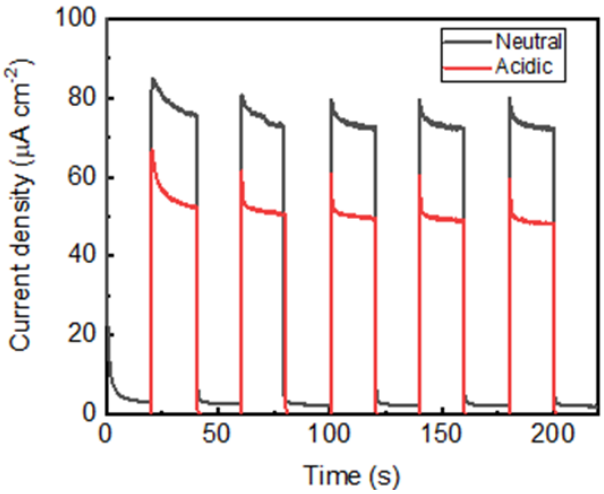

Fig. S25 Chronoamperometry: current density (on off illumination cycles) of CN_{M+mlm} electrode in different electrolytes neutral (0.5 M Na_2SO_4, pH 6.27), and acidic (0.5 M H_2SO_4, pH 0.27), plotted in black and red, respectively.

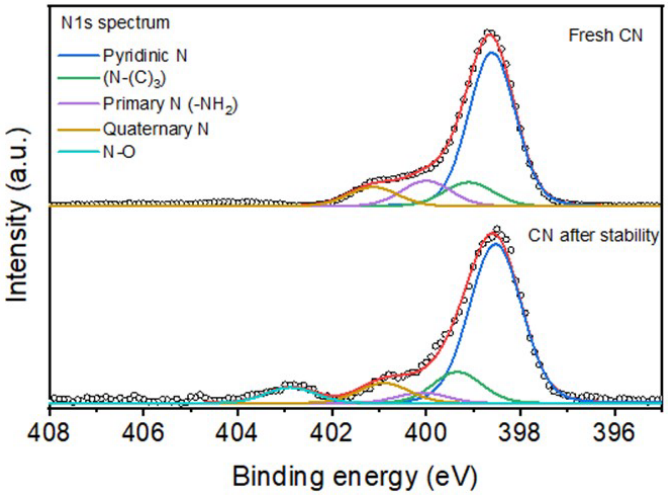

Fig. S26 N1s XPS spectra of CN_{M+mlm} electrode before and after PEC stability experiment.

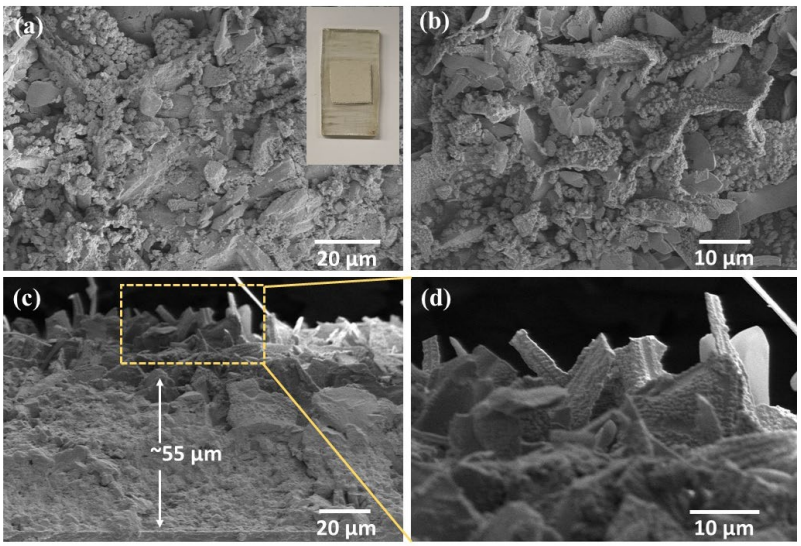

Fig. S27 SEM analysis of CN_{M+mlm} after a stability test. (a, b) Top-view images (inset of 'a' is photographic image of the electrode after 5 h stability test). (c, d) Cross-section image.

Electronic Supplementary Information References

[1] L. Abisdris, J. Tzadikov, N. Karjule, A. Azoulay, M. Volokh and M. Shalom, *Sustain. Energy Fuels*, 2020, **4**, 3879–3883.

[2] M. Nikookar, A. Rezaeifard, M. Jafarpour, K. V Grzhegorzhevskii and A. A. Ostroushko, *RSC Adv.*, 2021, **11**, 38862–38867.

[3] Y. Yang, J. Chen, Z. Mao, N. An, D. Wang and B. D. Fahlman, *RSC Adv.*, 2017, **7**, 2333–2341.

[4] G. Mark, S. Mondal, M. Volokh, J. Xia, M. Shalom, *Sol. RRL* **2022**, *2200834*, 1–9.

[5] N. Karjule, J. Barrio, A. Tashakory, M. Shalom, *Sol. RRL* **2020**, *4*, 2000017.

[6] J. Xia, N. Karjule, B. Mondal, J. Qin, M. Volokh, L. Xing, M. Shalom, *J. Mater. Chem. A* **2021**, *9*, 17855–17864.

[7] N. Karjule, L. Abisdris, A. Azoulay, M. Volokh, M. Shalom, *Adv. Energy Sustain. Res.* **2022**, *2200035*, 2200035.

[8] X. Wu, X. Wang, F. Wang, H. Yu, *Appl. Catal. B Environ.* **2019**, *247*, 70–77.

[9] Y. Huang, D. Li, Z. Fang, R. Chen, B. Luo, W. Shi, *Appl. Catal. B Environ.* **2019**, *254*, 128–134.

[10] Y. Zhou, W. Lv, B. Zhu, F. Tong, J. Pan, J. Bai, Q. Zhou, H. Qin, *ACS Sustain. Chem. Eng.* **2019**, *7*, 5801–5807.

[11] H. Liu, J. Liang, S. Fu, L. Li, J. Cui, P. Gao, F. Zhao, J. Zhou, *Colloids Surfaces A Physicochem. Eng. Asp.* **2020**, *591*, 124552.

[12] R. Ma, L. Dong, B. Li, T. Su, X. Luo, Z. Qin, H. Ji, *ChemistrySelect* **2018**, *3*, 5891–5899.

[13] K. L. Corp, C. W. Schlenker, *J. Am. Chem. Soc.* **2017**, *139*, 7904–7912.

[14] L. Cui, J. Song, A. F. McGuire, S. Kang, X. Fang, J. Wang, C. Yin, X. Li, Y. Wang, B. Cui, *ACS Nano* **2018**, *12*, 5551–5558.

[15] H. Schlomberg, J. Kröger, G. Savasci, M. W. Terban, S. Bette, I. Moudrakovski, V. Duppel, F. Podjaski, R. Siegel, J. Senker, R. E. Dinnebier, C. Ochsenfeld, B. V Lotsch, *Chem. Mater.* **2019**, *31*, 7478–7486.

[16] Y. Wang, Y. Zhang, S. Zhao, Z. Huang, W. Chen, Y. Zhou, X. Lv, S. Yuan,

Appl. Catal. B Environ. **2019**, *248*, 44–53.

[17] X. Jiang, L. Zhang, H. Liu, D. Wu, F. Wu, L. Tian, L. Liu, J. Zou, S. Luo, B. Chen, *Angew. Chem.* **2020**, *59*, 23112–23116.

[18] C. Li, H. Wu, D. Zhu, T. Zhou, M. Yan, G. Chen, J. Sun, G. Dai, F. Ge, H. Dong, *Appl. Catal. B Environ.* **2021**, *297*, 120433.

[19] J. Zhang, J. Chen, Y. Wan, H. Liu, W. Chen, G. Wang, R. Wang, *ACS Appl. Mater. Interfaces* **2020**, *12*, 13805–13812.

[20] L. Zhang, Z. Jin, S. Huang, X. Huang, B. Xu, L. Hu, H. Cui, S. Ruan, Y.-J. Zeng, *Appl. Catal. B Environ.* **2019**, *246*, 61–71.

[21] H. Zhang, J. Lin, Z. Li, T. Li, X. Jia, X. Wu, S. Hu, H. Lin, J. Chen, J. Zhu, *Catal. Sci. Technol.* **2019**, *9*, 502–508.

[22] Y. Yuan, Z. Shen, S. Wu, Y. Su, L. Pei, Z. Ji, M. Ding, *Appl. Catal. B Environ.* **2019**, *246*, 120–128.

[23] F. Yang, D. Liu, Y. Li, L. Cheng, J. Ye, *Appl. Catal. B Environ.* **2019**, *240*, 64–71.

[24] A. Hayat, N. Shaishta, I. Uddin, M. Khan, S. Kumar, B. Mane, A. Hayat, I. Ullah, A. Ur, T. Ali, G. Manjunatha, *J. Colloid Interface Sci.* **2021**, *597*, 39–47.

[25] T. Huo, G. Ba, Q. Deng, F. Yu, G. Wang, H. Li, *Appl. Catal. B Environ.* **2021**, *287*, 119995.

[26] C. Cheng, C. Dong, J. Shi, L. Mao, Y. Huang, *J. Mater. Sci. Technol.* **2022**, *98*, 160–168.

[27] Q. Li, L. Zhang, J. Liu, J. Zhou, Y. Jiao, X. Xiao, C. Zhao, Y. Zhou, S. Ye, B. Jiang, J. Liu, *Small* **2021**, *17*, 2006622.

[28] X. Zhou, B. Xu, J. Zhang, Q. Zhao, C. Li, H. Dong, X. Wang, J. Yang, *Int. J. Hydrogen Energy* **2021**, *46*, 38299–38309.

[29] J. Xia, N. Karjule, G. Mark, M. Volokh, H. Chen, M. Shalom, *Nano Res.* **2022**, *15*, 10148–10157.